Design of a Novel Bimanual Robotic System for Single-Port Laparoscopy

Marco Piccigallo, Umberto Scarfogliero, *Member, IEEE*, Claudio Quaglia, Gianluigi Petroni, Pietro Valdastri, *Member, IEEE*, Arianna Menciassi, *Member, IEEE*, and Paolo Dario, *Fellow, IEEE*

***Abstract*—This paper presents the design and fabrication of Single-Port lapaRoscopy bImaNual roboT (SPRINT), a novel tele-operated robotic system for minimally invasive surgery. SPRINT, specifically designed for single-port laparoscopy, is a high-dexterity miniature robot, able to reproduce the movement of the hands of the surgeon, who controls the system through a master interface. It comprises two arms with six degrees of freedom (DOFs) that can be individually inserted and removed in a 30-mm-diameter umbilical access port. The system is designed to leave a central lumen free during operations, thus allowing the insertion of other laparoscopic tools. The four distal DOFs of each arm are actuated by on-board brushless dc motors, while the two proximal DOFs of the shoulder are actuated by external motors. The constraints generated by maximum size and power requirements led to the design of compact mechanisms for the actuation of the joints. The wrist is actuated by three motors hosted in the forearm, with a peculiar differential mechanism that allows us to have intersecting roll–pitch–roll axes. Preliminary tests and validations were performed *ex vivo* by surgeons on a first prototype of the system.**

***Index Terms*—Bimanual robot, miniature robotic arm, minimally invasive surgery, robotic surgery, single-port laparoscopy (SPL).**

I. Introduction

LAPAROSCOPIC surgery is a standard in today's medicine. Surgical techniques of this kind consist of the use of stiff and long instruments that are inserted in the abdomen through small incisions, after having inflated the abdominal cavity, while an endoscope transmits the bidimensional images of the organs on a video screen. Although the patient benefits from the reduced invasiveness, the surgeon's sensory, and motor capabilities are limited [1]. The insertion points limit the freedom of movements of a rigid laparoscopic instrument to only four degrees of freedom (DOFs): this means that each reachable point inside the abdomen can only be approached with a fixed orientation of the instrument, and that some anatomical regions are not accessible. The insertion point acts as fulcrum constraint on the long, stiff instruments, thus causing nonintuitive effects on the tip movements, such as movement inversion and velocity scaling.

Manuscript received February 24, 2010; revised June 18, 2010; accepted September 7, 2010. Date of publication October 14, 2010; date of current version December 15, 2010. Recommended by Guest Editor K. Masamune. This work was supported by the European Commission in the framework of ARAKNES FP7 under European Project 224565.

The authors are with the CRIM Lab, Scuola Superiore Sant'Anna, Pisa 56025, Italy (e-mail: m.piccigallo@sssup.it; u.scarfogliero@sssup.it; c.quaglia@sssup.it; g.petroni@sssup.it; p.valdastri@sssup.it; a.menciassi@sssup.it; p.dario@sssup.it).

Color versions of one or more of the figures in this paper are available online at http://ieeexplore.ieee.org.

Digital Object Identifier 10.1109/TMECH.2010.2078512

In the past few years, novel surgical techniques have been progressing from research to clinical practice with the aim of further reducing invasiveness and access trauma. Natural orifices transluminal endoscopic surgery (NOTES) [2] is a totally scarless technique by which it is possible to reach the peritoneal cavity through a transluminal incision performed with flexible instruments inserted either from the mouth, the anus, or the vagina. Despite a clear esthetic benefit, the intentional perforation of a healthy organ and the current lack of a well-established method for closing such a perforation make NOTES effective mainly in the case of vaginal access [3], [4]. Additionally, at the moment NOTES is performed with traditional endoscopic instrumentation that is not specifically designed for this kind of surgery [5].

A novel technique that is halfway between traditional laparoscopic surgery and NOTES is single-port laparoscopy (SPL), which consists of a single incision at the umbilicus through which multiple instruments can be placed [6]. This seems to have more possibilities to be accepted as a standard practice in a short period since it allows a direct access to the abdominal cavity by exploiting a pre-existing scar, thus avoiding additional incisions on the patient's body. However, SPL has more limitations than the laparoscopic approach, because it does not allow triangulation from two different points, thus severely limiting the dexterity of the surgeon, although several ad hoc instruments have been developed and are already on the market [6], [7]. Furthermore, retraction of the organs is hampered, and this is another issue that led to research and development of novel devices and techniques [8].

The introduction of robotics in surgery generated a tremendous impact, with over 1000 surgical robots in regular clinical use worldwide, and research and development at over 100 universities [9]. In particular, the da Vinci Surgical System (Intuitive Surgical, Inc., Sunnyvale, CA) solved the dexterity problems of traditional laparoscopic surgery with a teleoperated master–slave manipulator that comprises a "master" console from which the surgeon controls the movements, while the "slave" part acts directly on the patient [10]. Thanks to an advanced cable-drive mechanism (EndoWrist, Intuitive Surgical, Inc., Sunnyvale, CA), the natural movement of the human wrist is almost completely restored on the teleoperated surgical instrument [11]. Additionally, stereoscopic vision enables the surgeon to perceive depth. These innovative features reduce by far the complexity of laparoscopic execution of certain procedures, such as suturing, still preserving the minimally invasive approach, with typically four incisions. Recently, the da Vinci Surgical System has been applied also to NOTES [12] and to

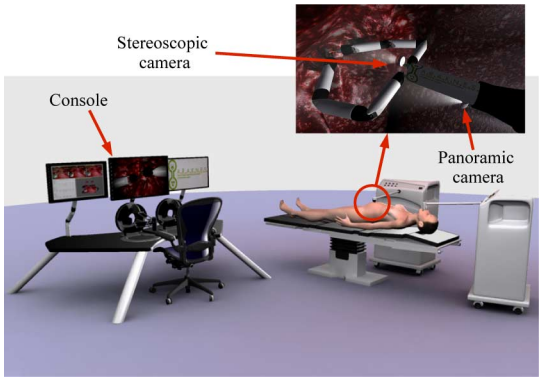

Fig. 1. 3-D simulation showing the concept of the bimanual robot for SPL.

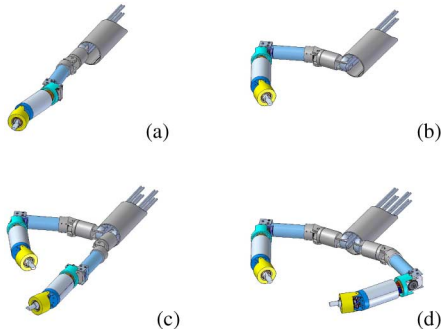

Fig. 2. Phases of insertion of the robotic arms, showing how two arms can fit through the umbilical access port (a) and (b) and be kept in working position by a central holder (c) and (d).

SPL [13], [14] demonstrating that both these procedures are feasible using the current robotic system, though, with considerable limitations [15].

Robotic systems designed specifically for NOTES and SPL approaches have the potential of making scar-less surgery effective and reliable, thus finally realizing its full potential and paving the way to the next generation of surgical robots. Several robotic solutions have already been specifically designed for NOTES [16]–[18]. However, the lack of a stable anchoring and the size constraint imposed by the endoluminal access prevent them to reach the same performance in terms of force and speed as the da Vinci Surgical System. Other robotic devices are being studied, designed specifically for SPL [19], [20]. A robotic system designed for SPL may benefit from both a direct and rigid link with an external support and a considerably large diameter of the access port. This approach has been pursued by the authors in designing a novel bimanual and modular robotic system to be used in single-port surgery. This paper presents the design and prototyping of Single-Port lapaRoscopy bImaNual roboT (SPRINT). In particular, the design of mechanisms and solutions that allow the actuation of two 6-DOF robotic arms through an umbilical access port is reported. Section II illustrates the concept of the system, while in Section III a detailed description of the robot is presented. In Section IV, the performances of the first prototype of single arm are discussed together with some test results. Section V draws the conclusion and underlines future developments.

II. The SPRINT Robotic System

SPRINT is a multiarm robot aimed at enabling bimanual interventions with a single access port (Fig. 1).

The robotic arms are introduced in the abdomen through a cylindrical access port. The navel is surgically considered as a natural scar and it can be used to gain access to the abdomen in a practically scar-less way. According to medical constraints, the maximum diameter achievable of the orifice is 30–35 mm [6]. The umbilical access port has been specifically designed to allow the insertion of each arm separately, and each arm could be removed in order to clean or replace the tool (Fig. 2).

The surgeon controls the robotic arms in a master–slave configuration through a dedicated console, and the robotic arms reproduce the movements of the surgeon's hands. The advantages of this robotic platform is that surgeon has more control on the operating room respect to the da Vinci system, while the resulting apparatus is much less bulky and could lead in the future to a rapid set-up of the operating room.

Up to four arms can be inserted: in addition to the two main arms, a stereoscopic-camera holder and, for example, a retractor could be introduced. A central lumen of 12 mm is left open after the insertion of the arms, and assistive tools could be inserted for additional tasks (e.g., hemostatic sponge, suturing needle, and wire). Each robotic arm has six active DOFs plus the gripper, arranged in a serial configuration, and it is designed for achieving a large workspace, necessary for completing surgical tasks while attached to the umbilical access port. As regards the desirable robotic arm diameter, keeping it in the range of 18 mm would allow us to extend the impact of the presented design from SPL to NOTES, following a similar approach to the one proposed in [17], where a 17-mm-diameter bimanual robot is introduced endoscopically through the esophagus to perform a NOTES cholecystectomy. For the same reason the total length of each robotic arm has been targeted to 120 mm. The limited size of the robot implies strong mechanical constraints in the design, taking into account the force and speed needed for executing a variety of surgical tasks. The arm would be inserted in the umbilical access port parallel to the axis of the insertion cylinder. A guiding rail could be used during the insertion to facilitate or automatize the insertion motion. As the arms reach the bottom of the umbilical port, they have to be rotated by 90°, reaching the operative configuration as shown in Fig. 2(c). This operation is allowed by a cable-driven joint placed at the base of the arm, operated by external motors. As described later, this joint is not present in the first robot prototype, mainly used for testing the design and dexterity of the arm itself. Guiding rails on which the robotic arms slide ensure the proper rigidity to the system.

The procedure for the insertion of the arms would consist of the following steps:

1) incision of the abdomen at the navel;
2) insertion of the umbilical access port with panoramic camera;
3) insertion of the stereoscopic camera supporting arm (not shown in Fig. 2);

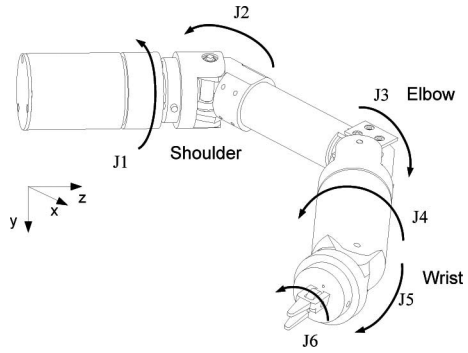

Fig. 3. Schematic drawing of one arm showing the kinematic configuration.

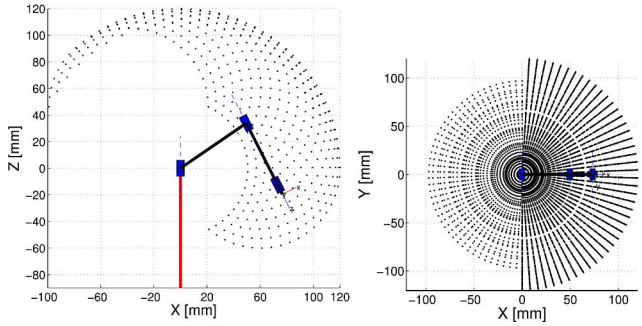

Fig. 4. 2-D graphical representation of the workspace of one robotic arm.

4) insertion of the first operative arm [Fig. 2(a)];
5) insertion of the second operative arm [Fig. 2(c)];
6) insertion of additional tools if needed.

In the design of the access port, it is fundamental to guarantee a safe removal of the robotic arms also in case of misfunctioning, and the possibility of folding the robot back into the introduction cylinder must not be precluded. Thus, the arms are back-drivable enough to be retrieved in case of failure inside the insertion port pulling them from outside.

The use of guiding rails on the insertion cylinder, and the design of the transmission system, allows the insertion of additional smaller arms on the upper and lower side. As previously indicated, one slot would be used for a small arm with a stereoscopic camera, while the other could be useful for retraction, for positioning lightening fibers or a camera, and for introducing sensors or additional tools. The whole system can be held by a positioner that keeps the introduction cylinder in fixed position during the operation.

The following sections present the design chosen for actuating six DOFs in a 18-mm-diameter arm, and the implemented mechanical solutions are described in detail.

III. System Description

As already described in Section II, the main part of the system comprises two arms for bimanual operations inside the abdomen. The robot is inserted through a single access port in the navel, with an incision of about 30–35 mm. Each arm is a 6-DOF manipulator in an anthropomorphic serial configuration. The arrangement of DOFs in the kinematic chain was chosen to match the workspace and dexterity required by surgeons that collaborated in defining these specifications. The distal DOFs used for positioning are roll–pitch–pitch, followed by a roll–pitch–roll compact spherical wrist with intersecting axes (Fig. 3); therefore, each point of the workspace can be reached with any orientation (Fig. 4). Being the abdomen inflated, the maximum distance (with the arm in the straight position) between the base of the arm and the point of intervention could be up to 275 mm, and we designed the arm accordingly [21].

The requirements for selecting actuators and designing the mechanisms have been evaluated considering the measurements reported in the literature. The typical forces that a laparoscopic device should withstand are reported in [22] and [23]. Performance, in terms of force and speed, of other teleoperated systems for surgery have also been taken into account and evaluated [10], [24]. Forces exerted on the tip do not usually exceed 5 N, while the mean gripping force needed is measured to be about 10 N. A speed of the joints of at least 360°/s is necessary for the slave robot in order to follow the surgeon's movement at the master interface [25].

The design has been carried out taking into account these requirements. Although some robots for SPL use a flexible transmission with external actuators, like those described in [19] and [20], a configuration featuring most of the motors embedded has been preferred for the SPRINT robot. Having a rigid transmission allows higher stiffness and the possibility of exerting higher torques. On the other hand, miniature cable/pulleys mechanisms are mostly suited for 3-DOF wrists, while for SPL, where both the arms are inserted through the same port, up to seven DOFs are required for each internal arm in order to perform traditional operations. Such a dexterity requires roll joints, which may be prohibitive to actuate by cable-driven mechanisms, resulting in a bulky and complex system. Moreover, the selected motors are already commonly used in dental applications, and are sterilizable on request.

The torque applied on the joints depends on the present position of the tip, but in the worst case the shoulder joint should be capable to generate a torque equal to the force applied on the end-effector times the sum of all the link lengths. This implies a value of power up to 4 W for the proximal joints and about 1 W for the wrist, considering feasible values for the link lengths (about 60 mm). However, small electric motors cannot exert the power needed to actuate the shoulder joint. Considering the strict size requirements, mainly on the diameter of the links (18 mm), it is not feasible to put all the six actuators inside the arm; hence, the motors operating the two proximal joints have been placed outside. Restrictions on the size and power of the external actuators are much less critical; however, mechanical power must be transmitted from the motors to the proximal joints by a rigid or flexible mechanical transmission. In the final design, as described in Section II, both the main arms should be introduced from a cylindrical tube and then the first link should be rotated by 90°, so that the link axis and tube axis are perpendicular (Fig. 2). A cable-driven transmission between external motors and joints $J1$ and $J2$ (with the notation of Fig. 3) is, therefore, the most suitable solution, according to the main

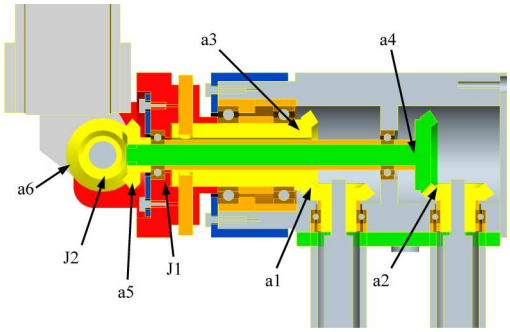

Fig. 5. Computer-aided design drawing of the shoulder mechanism.

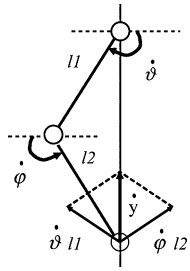

Fig. 6. Schematic of a planar 2-DOF robot that shows the relation between the rotational speed of the two links during a linear retraction motion.

concept of the system described in the previous section and depicted in Figs. 1 and 2. However, for the first prototype described in this paper, a rigid shaft transmission has been chosen in order to simplify the fabrication and to prove the concept of the proposed design.

A. Shoulder Mechanism

The mechanism that activates the two proximal joints (i.e., the shoulder) consists of a system of bevel gears arranged in a differential configuration (Fig. 5). Bevel gear $a1$ transmits the movement to the roll joint ($J1$), while bevel gear $a2$ transmits the movement to the pitch joint ($J2$). Being the two shafts of bevel gears $a3$ and $a4$ coaxial, the mechanism allows us to transmit the mechanical power to the pitch joint $J2$ overcoming the first roll joint $J1$, implying at the same time that the two movements are kinematically coupled.

Defining the gear ratio $N_{i,j}$ between two consecutive gears as

$$N_{i,j} = \frac{z_i}{z_j} \tag{1}$$

where z is the number of teeth, i and j are the leading and follower gears, the equations relating joint movements θ_{J1} and θ_{J2} to the rotation $\theta_{in,1}, \theta_{in,2}$, respectively, of the gears $a1, a2$ can be expressed as follows:

$$\begin{cases} \theta_{J1} = \theta_{in,1} N_{a1,a3} \\ \theta_{J2} = \theta_{in,2} N_{a2,a4} N_{a5,a6} - \theta_{in,1} N_{a1,a3} N_{a5,a6}. \end{cases} \tag{2}$$

The two input bevel gears $a1$ and $a2$ are actuated by two externally positioned dc motors (Faulhaber 2342). These are 18-W motors coupled with 43:1 gearheads, so that the two proximal joints can exert a torque of 700 N·mm at 540°/s.

As shown in Fig. 5, two long shafts, placed inside the insertion tube, are used to transmit mechanical power to the bevel gears $a1$ and $a2$. As discussed at the end of the previous section, this rigid transmission has been chosen only for the first prototype in order to simplify manufacturing and validate the shoulder mechanism. In the next prototype, currently under design, the same mechanism depicted in Fig. 5 will be used, but a different kind of transmission will be implemented to actuate gears $a3$ and $a4$: each gear will be connected to a cable-driven pulley by a purposely studied design. This will allow us to add a rotational joint while preserving the transmission of motion to the subsequent $J1$ and $J2$ joints from the external motors. The additional rotational joint will be required to rotate the arm in the operative position after the insertion (Fig. 2(b)).

B. Elbow Mechanism With On-Board Actuation

The elbow, corresponding to $J3$ in Fig. 3, is actuated by a brushless dc motor placed in the rigid link connecting $J2$ to $J3$. The motion is transmitted from the arm axis to the perpendicular joint axis by means of two bevel gears coupling the motion of forearm to the motor. The actuator is a Faulhaber 1226, able to provide 9 W of power within 12 mm diameter. The reduction gear ratio is 161:1; therefore, the motor is able to exert a torque of 360 N·mm at a speed of 1188°/s. The power and the reduction gear of the motor have been chosen in order to achieve a rotational speed double respect to the shoulder, while allowing the desired maximum force at the tip (5 N). The dimensioning criterion of double speed in the elbow allows us to keep a maximum linear speed of the tool along a straight line, which can be useful during the retraction motion. Fig. 6 shows a schematic 2-DOF manipulator, where for clarity rotational speeds $\dot{\varphi}$ and $\dot{\vartheta}$, respectively, of link 1 and link 2 are positive when bringing positive retraction motion $\dot{y}$. As in our case the two links (arm and forearm) measure about the same length, the motion is vertical when $\dot{\varphi} = \dot{\theta}$. The relative elbow rotational speed of link 2 with respect to link 1 is $\dot{\varphi}_r = \dot{\varphi} + \dot{\theta}$, and it becomes $\dot{\varphi}_r = 2\dot{\theta}$ during linear motion. Thus, the optimal performances can be achieved when the motor of the elbow is chosen for a reference speed that is twice the speed of the shoulder.

Regarding the range of motion of the elbow joint, it is essential that the maximum bending exceeds significantly 90°, in order to preserve the wide workspace, especially needed for bimanual operations. To allow a wide inward rotation, the elbow joint has been designed with the axis of rotation $J3$ not intersecting the motor axis (Fig. 7), but translated of a few millimeters. This also allows us to relief the motor shaft from the axial and radial forces created by the bevel gear, while shortening the link length. As can be noticed in Fig. 7, the motor shaft $s1$ rotates the spur gear $b1$ that leads the gear $b2$ and thus transmits the rotation to the forearm through the couple of bevel gears $b3$ and $b4$. In this way the elbow can reach an inward motion of $+130°$, while allowing an extension of $-55°$. Considering $N_{b1,b4}$ as the gear ratio of the whole mechanism shown in Fig. 7, the angular displacement

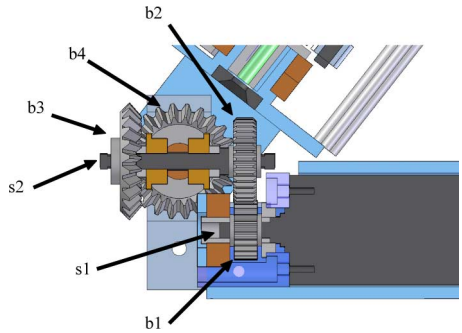

Fig. 7. Structure of the elbow allows wide range of motion and reduce the articulation length.

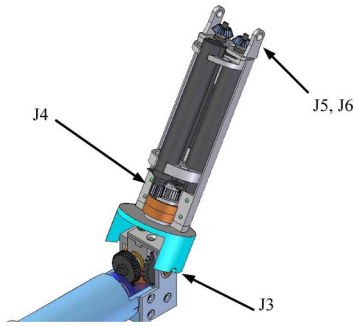

Fig. 8. Disposition of the three motors in the forearm for the wrist actuation.

θ_{J3} of the joint can be written as follows:

$$\theta_{J3} = N_{b1,b4}\theta_{\text{in},3} \tag{3}$$

where $\theta_{\text{in},3}$ is the angular position of input gear $b1$.

C. The Wrist Mechanism With On-Board Actuation

As introduced previously, the elbow and wrist of the robotic arm have on-board actuation. The forearm hosts three Maxon EC6 brushless motors of 6 mm in diameter, and a mean power of 1.2 W each, actuating the distal 3 DOFs (roll–pitch–roll) of the wrist. Each motor is equipped with an encoder and a 221:1 reduction gear head, providing a nominal torque of 50 N·mm, and a speed of 600°/s. The three axes are intersecting thanks to a particular design of the transmission mechanism. In the 18 mm diameter, the three motors are aligned along the forearm axis (Fig. 8).

While one motor actuates directly the roll *J4*, the other two are coupled in a differential mechanism that actuates the pitch *J5* and the roll *J6*. Due to the size constraints, the motors are mounted with the axes parallel to the forearm. The joint angle θ_{J4} can be simply computed as follows:

$$\theta_{J4} = N_4\theta_{in,4} \tag{4}$$

where N_4 is the reduction ratio of joint $J4$. As shown in Fig. 9, the differential mechanism is composed of a triplet of three bevel gears for each motor. The two triplets are coupled by spur gears *c7*, *c8*, *c9* that build up the differential. The gears *c2* and *c5* are idle on the shaft *s5*, while gears *c3* and *c6* are rigidly attached respectively to spur gears *c7* and *c8*. The spur gear *c9* rotates the

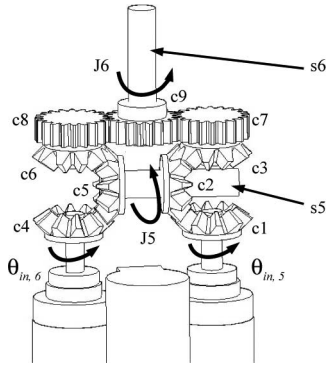

Fig. 9. Differential mechanism used for the two distal DOFs of the robotic arm.

shaft *s6* resulting in the roll motion *J6*. When the two motors rotate in the same direction with the same speed, only the pitch *J5* is actuated along the shaft *s5*, while the roll *J6* is actuated when the two motors rotate in opposite direction and the same speed.

As previously described for the shoulder mechanism, the equations relating pitch and roll rotations to motor's motion can be derived as function of the motor's rotations $\theta_{in,5}$ and $\theta_{in,6}$. An equal gear ratio has been selected for the two triplets of bevel gears composing the differential, and for the two spur-gear couples

$$\begin{cases} N_b = N_{c4,c5} = N_{c1,c2} = N_{c6,c5} = N_{c3,c2} \\ N_g = N_{c7,c9} = N_{c8,c9}. \end{cases} \tag{5}$$

Thus, θ_{J5} and θ_{J6} can be derived as follows:

$$\begin{cases} \theta_{J5} = \dfrac{\theta_{in,5} - \theta_{in,6}}{2} N_b \\ \theta_{J6} = \dfrac{\theta_{in,5} + \theta_{in,6}}{2} N_g. \end{cases} \tag{6}$$

D. Overview of the Control Architecture

For the first prototype of the robot, the PHANTOM Omni (SensAble Technologies, Woburn, MA) has been chosen as the master interface because it can sense the position in 6 DOFs. Four externally positioned EPOS 24/1 position controllers by Maxon are used to drive the four internal motors, while two Faulhaber MCDC 3006C controllers are used to drive the external motors. Encoders embedded in the motors provide the current relative angular position of each motor shaft (θ_{mi}), thus enabling a position control. All the drivers communicate via CAN-Bus with a Linux-based personal computer (PC). A C++ software that runs on the PC reads the position and orientation of the master from the IEEE 1394 interface and sends the desired positions of the motors to the controllers through a CAN-PCI card (PEAK-System Technik, Germany). Each motor controller implements a local closed-loop by means of a proportional-integral-derivative position control. The workspace of the master is thus mapped on the workspace of the slave.

At each instance of the control loop the absolute position and orientation of the master are acquired and then computed relatively to the starting position, chosen by the user at the

beginning of the procedure, as follows:

$$\boldsymbol{R}_{M\mathrm{rel}} = \boldsymbol{R}_{M\mathrm{start}}^{T} \cdot \boldsymbol{R}_{M} \tag{7}$$

where $\boldsymbol{R}_M$ is the absolute rotation matrix of the master, $\boldsymbol{R}_{M\mathrm{start}}$ is the rotation matrix of the starting position, and $\boldsymbol{R}_{M\mathrm{rel}}$ is the rotation relative to the starting position. The desired 3×3 rotation matrix of the end-effector with respect to the base frame is thus computed as follows:

$$\boldsymbol{R}_{6}^{0} = \boldsymbol{R}_{6\mathrm{start}}^{0} \cdot \boldsymbol{R}_{M\mathrm{rel}} \tag{8}$$

where $\boldsymbol{R}_{6\mathrm{start}}^{0}$ is the rotation matrix of the starting position of the end-effector. Similarly, the desired position of the end-effector is computed as follows:

$$\boldsymbol{P} = \boldsymbol{P}_{M\mathrm{rel}} + \boldsymbol{P}_{\mathrm{start}} \tag{9}$$

where $\boldsymbol{P}_{M\mathrm{rel}}$ is the position of the master, relative to the its starting position $\boldsymbol{P}_{M\mathrm{start}}$, and $\boldsymbol{P}_{\mathrm{start}}$ is the starting position of the slave's end-effector. The vector of joint angles $\boldsymbol{\theta}_J = \{\theta_{J1} \cdots \theta_{J6}\}$ is then computed by inverting the kinematics of the robot. As the 6 DOFs arm has a spherical wrist, the calculation of the first three joint angles can be decoupled from that of the last three. The position of the wrist center, $\boldsymbol{P}_w$, can be determined as follows:

$$\boldsymbol{P}_w = \boldsymbol{P} - \boldsymbol{z}_6 \cdot d \tag{10}$$

where d is the distance between the wrist center and the tool and $\boldsymbol{z}_6$ is the unit vector that represents the z-axis of the tool reference frame. $\boldsymbol{P}_w$ can be written as a function of the joint angles θ_{J1}, θ_{J2}, and θ_{J3}, while the three joint angles can be computed by inverting the kinematics. Then, the last three joint angles are computed by solving the following equation:

$$\boldsymbol{R}_{6}^{3} = \boldsymbol{R}_{3}^{0^T} \cdot \boldsymbol{R}_{6\mathrm{start}}^{0} \cdot \boldsymbol{R}_{M\mathrm{rel}}. \tag{11}$$

The vector of the angular positions of the output shafts of the motors $\boldsymbol{\theta}_{in} = \{\theta_{in,1} \ldots \theta_{in,6}\}$ is then computed by inverting the systems of (2)–(4), and (6). The vector $\boldsymbol{\theta}_m = \{\theta_{m1} \ldots \theta_{m6}\}$ of the target angular positions of each motor is transmitted to the motor drivers and it is computed as follows:

$$\begin{cases} \theta_{m1} = \dfrac{\theta_{J1}}{N_{m1}N_{a1,a3}} \\ \theta_{m2} = \dfrac{\theta_{J2} + \theta_{J1}N_{a5,a6}}{N_{m2}N_{a2,a4}N_{a5,a6}} \\ \theta_{m3} = \dfrac{\theta_{J3}}{N_{m3}N_{3}} \\ \theta_{m4} = \dfrac{\theta_{J4}}{N_{m4}N_{4}} \\ \theta_{m5} = \dfrac{N_b\theta_{J6} + N_g\theta_{J5}}{N_bN_gN_{m5}} \\ \theta_{m6} = -\dfrac{-N_b\theta_{J6} + N_g\theta_{J5}}{N_gN_{m6}N_b} \end{cases} \tag{12}$$

where N_{mi} is the gearhead ratio of motor i.

IV. Preliminary Tests and Performance

Characteristics and performance values of the robotic arm are summarized in Table I. A single arm has been fabricated

TABLE I
Performance

	Desired Performance	First Prototype
Speed	1 m/s	1 m/s
Force	5 N in every direction	5 N in every direction
Max. Diameter	18 mm	23 mm
Total Length	120 mm	142 mm

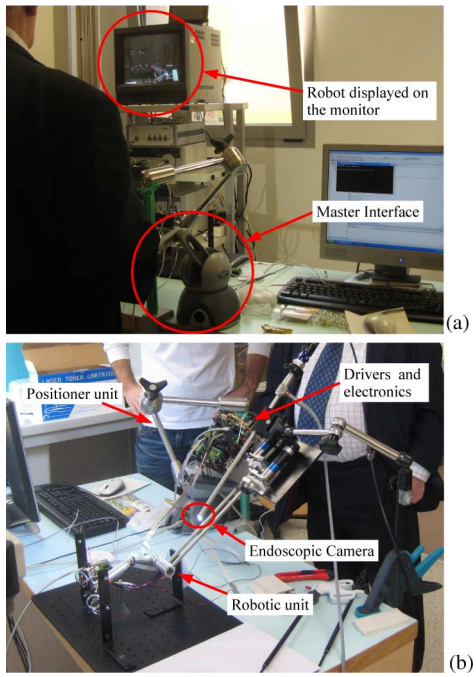

Fig. 10. Picture of the testbed for the pick-and-place exercise.

to validate the concept of the proposed design and to assess the validity of the system's dimensioning. The total length of this first prototype, from the first joint to the base of the tool, is 142 mm: 64 mm for the arm, 70 mm for the forearm, and 8 mm for the distal link. The maximum diameter of the arm is 23 mm, despite the link between the shoulder and the elbow is 16 mm in diameter. The diameter can be reduced by using higher precision computer-numerical-control (CNC) machining in the fabrication of some parts. Joint limits are $[-90°, 90°]$ for $J1$, $[-45°, 90°]$ for $J2$, $[-55°, 130°]$ for $J3$, $[0, 360°]$ for $J4$ and $[-60°, 60°]$ for $J5$ and $[0, 360°]$ for $J6$. Each joint of the first prototype has a backlash of about 2° that causes an error of about 8 mm of the end-effector (measured with a magnetic localization system). We expect to reduce this value to 2 mm maximum in the next prototype by using more precise couplings and a higher teeth number in the gears. Considering each joint at its nominal speed, the tool linear speed is around 1 m/s, depending on the robot configuration, while the maximum force exerted has been measured to be 5 N. This is a preliminary confirmation that the proposed design meets the requirements we adopted at the beginning of the design phase.

Pick-and-place tests have been carried out in which the prototype has been used by six people (five engineers and an experienced surgeon). A setup has been prepared with some rings and

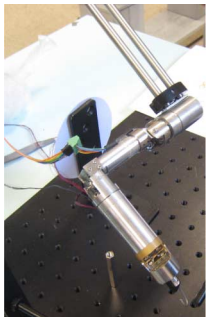

Fig. 11. Close-up picture of the SPRINT arm prototype.

holders in order to verify the dexterity of the arm in a master–slave teleoperated configuration. The aim of the exercise was to pick up a ring with the robotic arm from one ring holder and place it on another one. The distance between the two ring holders is 90 mm in the horizontal direction and 60 mm in the vertical one. Each tester was asked to perform the exercise watching the testbed scene on a video display as captured by an endoscopic camera (Fig. 10), positioned in the same configuration as in a real surgical intervention. A hook-shaped tool has been used as end-effector for these preliminary trials (Fig. 11), as the exercises were limited to the validation of the robotic-arm design and actuation. For the next prototype, a closing gripper will be developed. Testers of the system performed 10 pick-and-place tasks and they needed an average time of 25 s to move one ring from one stick to another, without any specific previous training on the SPRINT arm. Based on these encouraging results, we can envisage a quite fast learning curve for operating the system. However, additional extensive tests are required in order to further support this conclusion. The average latency between the movement acquired at the master side and the response of the robotic platform is about 16 ms. This value was computed by comparing the desired trajectory, imposed by the user on the master interface, with the readings of the motor encoders. In particular, such a total delay time includes the reading of master position, the computation of inverse kinematics, transmission of the target positions to each motor drivers over the CAN-Bus, and the low-level closed loops on motor positions. Regarding the electromechanical bandwidth of the robotic arm, a value of 5 Hz has been estimated by a model of the system.

V. Conclusion and Future Works

In this paper, a novel robotic platform named SPRINT for SPL in a master–slave configuration has been presented. To the best of the authors' knowledge, this is the first bimanual teleoperated robot purposely designed for an umbilical SPL access that has been reported so far. The system allows high dexterity, thanks to 6 DOFs for each arm, and can exert 5 N force on the tip while moving at a speed comparable to the surgeon's hand. Each arm can be introduced and removed separately, thus allowing us to change the surgical instrument on the fly. Two additional smaller arms can be inserted in the same access port. A first single-arm prototype of the design described in the paper has been fabricated, assembled and tested in a pick-and-place exercise. Future works will address a reduction in robot size and diameter. It is already possible to reduce the diameter of some links from current 23 mm to 18 mm by using high-precision CNC machining. The next step will also involve the design of cable-transmission mechanisms in the shoulder, in order to facilitate the insertion and positioning of the arms in the operative configuration. Tool exchange during operations and the durability of the platform will also be investigated in future developments and extensive tests. A six-axis load cell, such as the 17 mm diameter Nano 17 (ATI, Apex, NC), will be placed in between the tool and the wrist in order to enable both force feedback and position-force teleoperation [26], [27]. Furthermore, custom embedded electronics will be designed and integrated inside the arm and forearm in order to improve the performance of the control loop and to minimize the number of external cables. An improvement in the latency can be achieved by moving the control system to a real-time dedicated operative system and by adopting a communication faster than the CAN-Bus. In conclusion, despite a lot of work is still ahead of us before the final deployment of the complete platform, the design of a robotic system for umbilical SPL access may pave the way to the next generation of surgical robots, pursuing a scar-less approach for the sake of a faster recovery and an improved cosmetic effect for the patient.

Acknowledgment

The authors would like to thank N. Funaro, A. Melani, G. Favati, and C. Filippeschi for prototype manufacturing and also they are grateful to medical doctors A. Cuschieri, M.O. Schurr, and A. Peri for their medical advice.

References

[1] H. G. Stassen, C. A. Grimbergen, and J. Dankelman, "Introduction to minimally invasive surgery," in *Engineering for Patient Safety: Issues in Minimally Invasive Procedures*. Boca Raton, FL: CRC Press, 2004, pp. 2–18.

[2] A. N. Kalloo, V. K. Singh, S. B. Jagannath, H. Niiyama, S. L. Hill, C. A. Vaughn, C. A. Magee, and S. V. Kantsevoy, "Flexible transgastric peritoneoscopy: A novel approach to diagnostic and therapeutic interventions in the peritoneal cavity," *Gastrointest. Endosc.*, vol. 60, no. 1, pp. 114–117, Jul. 2004.

[3] G. Buess and A. Cuschieri. (2007, Jun.). Raising our heads above the parapet: Es not notes. *Surg. Endosc.* vol. 21, no. 6, pp. 835–837. [Online]. Available: http://dx.doi.org/10.1007/s00464-007-9437-z

[4] S. Horgan, J. P. Cullen, M. A. Talamini, Y. Mintz, A. Ferreres, G. R. Jacobsen, B. Sandler, J. Bosia, T. Savides, D. W. Easter, M. K. Savu, S. L. Ramamoorthy, E. Whitcomb, S. Agarwal, E. Lukacz, G. Dominguez, and P. Ferraina. (2009, Jul.). Natural orifice surgery: Initial clinical experience. *Surg. Endosc.* vol. 23, no. 7, pp. 1512–1518. [Online]. Available: http://dx.doi.org/10.1007/s00464-009-0428-0

[5] G. Spaun and L. L. Swanström, "Quo vadis NOTES?," *Eur. Surg.*, vol. 40, no. 5, pp. 211–219, 2008.

[6] M. Neto, A. Ramos, and J. Campos, "Single port laparoscopic access surgery," *Tech. Gastrointestinal Endosc.*, vol. 11, pp. 84–93, unskip 2009.

[7] J. R. Romanelli and D. B. Earle. (2009, Jul.). Single-port laparoscopic surgery: An overview. *Surg. Endosc.* [Online]. *23(7)*, pp. 1419–1427. Available: http://dx.doi.org/10.1007/s00464-009-0463-x

[8] M. Ryou and C. C. Thompson. (2009, Feb.). Magnetic retraction in natural-orifice transluminal endoscopic surgery (notes): Addressing the problem of traction and countertraction. *Endoscopy* [Online]. *41(2)*, pp. 143–148. Available: http://dx.doi.org/10.1055/s-0028-1119454

[9] J. S. Dai, "Surgical robotics and its development and progress," *Robotica*, vol. 28, no. 2, p. 161, 2010.

[10] A. Madhani, "Design of teleoperated surgical instruments for minimally invasive surgery," Ph.D. dissertation, Dept. Mech. Eng., Massachussets Inst. Technol., Cambridge, 1998.
[11] J. H. Palep, "Robotic assisted minimally invasive surgery," *J. Minimal Access Surg.*, vol. 5, no. 1, pp. 1–7, 2009.
[12] G.-P. Haber, S. Crouzet, K. Kamoi, A. Berger, M. Aron, R. Goel, D. Canes, M. Desai, I. S. Gill, and J. H. Kaouk, "Robotic notes (natural orifice translumenal endoscopic surgery) in reconstructive urology: Initial laboratory experience," *Urology*, vol. 71, no. 6, pp. 996–1000, 2008.
[13] W. M. White, G.-P. Haber, R. K. Goel, S. Crouzet, R. J. Stein, and J. H. Kaouk, "Single-port urological surgery: Single-center experience with the first 100 cases," *Urology*, vol. 74, no. 4, pp. 801–804, 2009.
[14] R. A. Joseph, A. C. Goh, S. P. Cuevas, M. A. Donovan, M. G. Kauffman, N. A. Salas, B. Miles, B. L. Bass, and B. J. Dunkin. (2009, Dec.). "Chopstick surgery: A novel technique improves surgeon performance and eliminates arm collision in robotic single-incision laparoscopic surgery," *Surg. Endosc.*, [Online]. Available: http://dx.doi.org/10.1007/s00464-009-0769-8
[15] W. M. White, G.-P. Haber, and J. H. Kaouk, "Robotic single-site surgery," *Curr. Opin. Urol.*, vol. 20, no. 1, pp. 86–91, 2010.
[16] D. Canes, A. Lehman, S. Farritor, D. Oleynikov, and M. Desai, "The future of NOTES instrumentation: Flexible robotics and *in vivo* minirobots," *J. Endourol.*, vol. 23, no. 5, pp. 787–792, 2009.
[17] A. Lehman, J. Dumpert, N. Wood, L. Redden, A. Visty, S. Farritor, B. Varnell, and D. Oleynikov, "Natural orifice cholecystectomy using a miniature robot," *Surg. Endosc.*, vol. 23, no. 2, pp. 260–266, 2009.
[18] S. J. Phee, S. C. Low, Z. L. Sun, K. Y. Ho, W. M. Huang, and Z. M. Thant, "Robotic system for no-scar gastrointestinal surgery," *Int. J. Med. Robot. Comput. Assist. Surg.*, vol. 4, no. 1, pp. 15–22, 2008.
[19] D. Q. Larkin, T. Cooper, E. F. Duval, A. MC-Grogan, C. J. Mohr, D. J. Rosa, B. M. Schena, D. C. Shafer, and M. R. Williams, "Minimally invasive surgical system," U.S. Patent WO2007146987, Jun. 2006.
[20] K. Xu, R. Goldman, J. Ding, P. Allen, D. Fowler, and N. Simaan, "System design of an insertable robotic effector platform for single port access (spa) surgery," in *Proc. 2009 IEEE/RSJ Int. Conf. Intell. Robots Syst. (IROS2009)*, pp. 5546–5552.
[21] P. Berkelman and J. Ma, "A compact, modular, teleoperated robotic minimally invasive surgery system," in *Proc. First IEEE/RAS-EMBS Int. Conf. Biomed. Robot. Biomechatron. (BioRob 2006)*, Feb., pp. 702–707.
[22] J. D. Brown, J. Rosen, L. Chang, M. Sinanan, and B. Hannaford, "Quantifying surgeon grasping mechanics in laparoscopy using the blue dragon system," *Med. Meets Virtual Reality*, vol. 13, pp. 34–36, 2004.
[23] C. Richards, J. Rosen, B. Hannaford, C. Pellegrini, and M. Sinanan, "Skills evaluation in minimally invasive surgery using force/torque signatures," *Surg. Endosc.*, vol. 14, pp. 791–798, 2000.
[24] M. Cavusoglu, "Telesurgery and surgical simulation: Design, modeling, and evaluation of haptic interfaces to real and virtual surgical environments," Ph.D. dissertation, Dept. Electr. Eng. Comput. Sci., Univ. of California, Berkeley, 2000.
[25] F. Cavallo, G. Megali, S. Sinigaglia, O. Tonet, and P. Dario, "A biomechanical analysis of surgeon's gesture in a laparoscopic virtual scenario.," *Stud. Health Technol. Inf.*, vol. 119, pp. 79–84, 2006.
[26] M. Mitsuishi, N. Sugita, and P. Pitakwatchara, "Force-feedback augmentation modes in the laparoscopic minimally invasive telesurgical system," *IEEE/ASME Trans. Mechatronics*, vol. 12, no. 4, pp. 447–454, Aug. 2007.
[27] N. Zemiti, G. Morel, T. Ortmaier, and N. Bonnet, "Mechatronic design of a new robot for force control in minimally invasive surgery," *IEEE/ASME Trans. Mechatronics*, vol. 12, no. 2, pp. 143–153, Apr. 2007.

Marco Piccigallo received the M.Sc. degree in mechanical engineering from the University of Pisa, Pisa, Italy, in 2003, and the Ph.D. degree in biorobotics science and engineering jointly from the IMT Institute for Advanced Studies, Lucca, Italy, and the Scuola Superiore Sant'Anna, Pisa, in 2008.

Since 2004, he has been with the CRIM Lab, Scuola Superiore Sant'Anna. His current research interests include biomedical robotics and computer-assisted surgery.

Umberto Scarfogliero (M'06) received the Master's degree in mechanical engineering from the Politecnico di Milano, Milan, Italy, in 2004, and the Ph.D. degree in biorobotics science and engineering jointly from the Scuola Superiore Sant'Anna, Pisa, Italy, and the IMT Institute for Advanced Studies, Lucca, Italy in 2008.

Since 2005, he has been with the CRIM Lab, Scuola Superiore Sant'Anna di Pisa, where he is involved in the design of miniature legged robots. His research interests include mechanism design and optimization of surgical robotics.

Claudio Quaglia received the Master's degree in mechanical engineering from the University of Pisa, Pisa, Italy, in 2005. His degree thesis focused on the employment of a triaxial accelerometer for tool condition monitoring in automatic machining. Since 2006, he has been working toward the Ph.D. degree in bioengineering at the Scuola Superiore Sant'Anna, Pisa.

His current research interests include medical robotics and micromechanical systems.

Gianluigi Petroni was born in 1984 in Lucca, Italy. He received the M.Sc. degree in biomedical engineering from the University of Pisa, Pisa, Italy, in 2009. He is currently working toward the Ph.D. degree in microbiorobotics at the Scuola Superiore Sant'Anna, Pisa.

His current research interests include biorobotics and teleoperated control systems.

Pietro Valdastri (M'05) received the Master's degree in electronic engineering (Hons.) from the University of Pisa, Pisa, Italy, in 2002, and the Ph.D. degree in bioengineering from the Scuola Superiore Sant'Anna, Pisa, in 2006.

He is currently an Assistant Professor of Biomedical Robotics at the Scuola Superiore Sant'Anna, where he is engaged in research on implantable robotic systems and active capsule endoscopy. He is involved in several European projects regarding the development of minimally invasive and wireless biomedical devices.

Arianna Menciassi (M'00) received the Master's degree in physics from the University of Pisa, Pisa, Italy, in 1995, and the Ph.D. degree from the Scuola Superiore Sant'Anna, Pisa, in 1999.

She is currently an Associate Professor of Biomedical Robotics at the Scuola Superiore Sant'Anna. Her current research interests include biomedical micro- and nanorobotics for the development of innovative devices for surgery, therapy, and diagnostics. She is the coauthor of more than 130 international papers, about 70 in ISI journals, and of five book chapters on medical devices and microtechnologies.

Paolo Dario (F' 02) received the Master's degree in mechanical engineering from the University of Pisa, Pisa, Italy, in 1977.

He is a Professor of Biomedical Robotics at the Scuola Superiore Sant'Anna, Pisa, where he supervises a team of about 150 young researchers. His current research interests include biorobotics, including mechatronic and robotic systems for rehabilitation, prosthetics, surgery, and microendoscopy. He is the author of more than 160 ISI journal papers, many international patents, and several book chapters on medical robotics.

Dr. Dario is a recipient of the Joseph Engelberger Award as a Pioneer of Biomedical Robotics.